Modeling surface defects in fused silica optics for laser wave propagation

A. Bourgeade,[1,*] T. Donval,[1] L. Gallais,[2] L. Lamaignère,[1] and J.-L. Rullier[1]

[1]*CEA-CESTA, 15 Avenue des Sablières, CS 60001, F33116 Le Barp Cedex, France*
[2]*Aix-Marseille Université, Centrale Marseille, CNRS, Institut Fresnel, 13013 Marseille, France*
**Corresponding author: antoine.bourgeade@cea.fr*

Received January 7, 2015; revised February 16, 2015; accepted February 18, 2015;
posted February 19, 2015 (Doc. ID 232068); published March 19, 2015

Modulation of the laser intensity caused by surface defects on optical components is a main concern for high-power lasers. Among the consequences of this effect, the laser damage occurrence can be magnified on the downstream components in the laser chain. In order to understand the impact of defects on wave propagation, a specific numerical approach has been developed. The defects are modeled as phase perturbations that are used as inputs in either a 1D axi-symmetric code based on finite differences or a 2D code that uses fast Fourier transform. The computations are then used to evaluate the laser intensity modulations generated by CO_2 laser-induced defects at the surface of fused silica optics. A dedicated damage experiment at 355 nm has been carried out for various defect dimensions. Consistent results are found between experiments and simulations, both on the quantitative values of magnitude and positions of the modulations. This study proves that, for short propagation distances, it is necessary to use the exact shape of the defect in the simulations, especially the complex rim structure characteristic of CO_2 laser craters.

OCIS codes: (050.1970) Diffractive optics; (000.4430) Numerical approximation and analysis; (140.3330) Laser damage.
http://dx.doi.org/10.1364/JOSAB.32.000655

1. INTRODUCTION

In the context of laser-induced damage of optical components, local CO_2 laser treatment is an effective method that prevents the growth of laser damage in a fused silica surface [1–4]. As a consequence of thermal treatment with the CO_2 laser to eliminate the fractured matter, a crater may be generated at the surface [5] as a residual stress field near the mitigated sites [6]. Based on experimental and numerical studies, additional laser heating was proposed to reduce this stress [7]. Despite the effectiveness of this process, a raised rim is often formed at the crater edge due to mass movement of silica at high temperatures outward from the low viscosity central region [8]. This outer rim can reach a height of several micrometers and result in the intensification of transmitted ultraviolet (UV) light that may damage the downstream optical components [9,10]. When the rim is located in the front surface of the optical component, the laser intensification could damage the rear surface of this same optical component [11]. There have been some papers dealing with the defect interaction with an incident laser beam: the intensity distribution has been numerically simulated around cracks [12] or spherical defects [13] with a finite element or FDTD approach. Light intensity modulations caused by opaque or transparent obstacles (e.g., dust, contaminants) [14,15] or damage sites [16] have also been addressed for millimetric propagation by use of Fresnel diffraction theory. Few theoretical studies have focused on the electrical field modulation of mitigated sites [9,17]. In these works, due to the resemblance between crater and a Gaussian shape, model defects (noted MD) used are commonly defined as having a perfect Gaussian profile [11]. However, only a few comparisons with experiments permit the validation of theoretical works considering real craters. In this study, the diffraction patterns at a discrete distance downstream from the front face mitigated site are first numerically simulated and then compared with experimental data.

To estimate the impact of a fused silica surface defect on UV laser beam propagation, we have developed 1D and 2D numerical codes. The two codes resolve the paraxial wave propagation equations. The 1D code is axi-symmetric and based on finite differences, while the 2D code uses a fast Fourier transform (FFT). The 1D approach allows us to follow the exact evolution of the electric field all along the distance of propagation. Nevertheless, the parabolic character of its equations limits the use of this approach to short distances. We have thus implemented a complementary 2D approach that gives the diffraction pattern at any distance. In order to validate numerical simulations, laser damage experiments have been carried out at 355 nm on mitigated sites taking into account the measured profile. These sites include different outer rims, which were located on the front face of the optical component. The occurrence or lack of occurrence of damage events on the rear face is determined at different laser fluences. A damage probability is then deduced and compared to the probability measured without a mitigated site, i.e., the intrinsic damage probability of the optical component. Comparison between the two probabilities, more precisely the fluences associated with them, is the method we have chosen to evaluate the amplification factor due to the outer rim. The comparison of this factor with the correspondent numerical result shows good correlation that validates our approach. We also observe that damage patterns on the rear face match those predicted by simulation.

The present paper is organized as follows. Section 2 deals with the numerical approach where the 1D and 2D codes are introduced independently. Section 3 presents the experimental procedure, which gives the estimation of the amplification factor (noted C) and the diameter of the damage patterns (noted ∅). The comparison between calculations and experimental results is presented in Section 4, which describes the numerical approach that permits us to determine the impact of fused silica surface defects on laser beam propagation.

2. NUMERICAL APPROACH

This part details the numerical approach we carry out to better understand the effect of fused silica surface defects on UV laser beam propagation. This work is divided into five parts and has been developed for monochromatic continuous waves, i.e., waves with a time-independent envelope. First, a CO_2-laser-induced crater at the surface of fused silica used as a test case for the approach is characterized. Then, the profile of this model defect (MD) is introduced in a code solving 2D or 3D Maxwell equations [18] for a short propagation (just a few micrometers beyond the MD) in order to determine the consequence of the MD on the laser beam intensity and phase. In the third part, the evolution of the wave envelope has been computed for longer propagation distances with a code solving the axi-symmetric 1D transverse propagation equation. This approach shows that a phase perturbation is a sufficient way to introduce an MD into the modeling of the laser beam propagation. In the fourth part, this conclusion is used in the general case: the 2D transverse approach solves the corresponding 3D envelope equation. Eventually, the case of a Gaussian beam illumination is taken into account for realistic comparison to dedicated laser damage experiments.

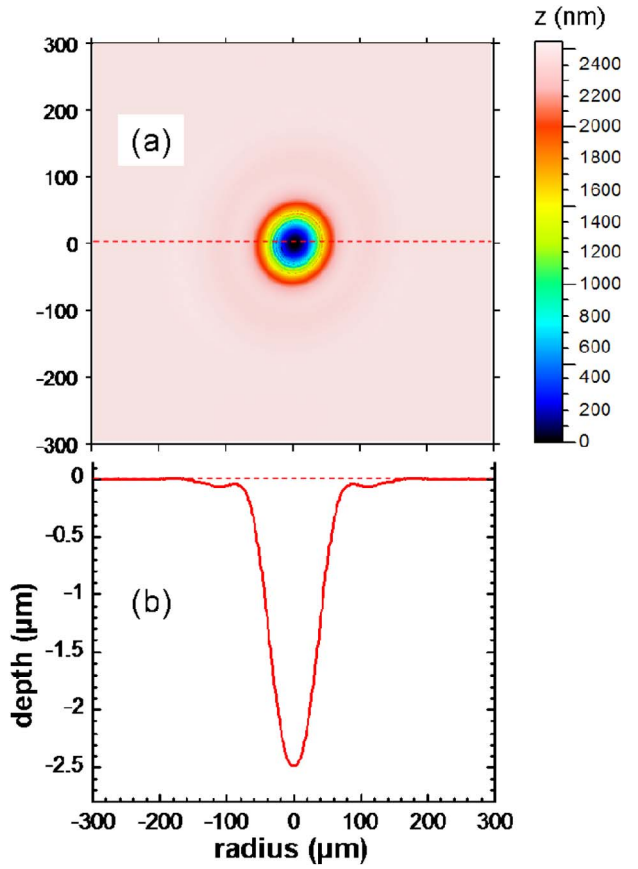

Fig. 1. Analysis by interferential microscopy of a site heated during 100 ms with a CO_2 laser power of 5.3 W. (a) 3D map. (b) Profile crossing the deepest zone along the dashed line.

A. Model Defect

For testing our numerical simulation, we used a crater as an MD noted MD_{test}. The crater has been realized with CO_2 laser irradiation on a fused silica sample, with an exposure time of 100 ms and a power of 5.3 W, in the experiment described in [1]. The site was characterized by white light interferometry; Fig. 1 shows a 3D view together with a profile crossing the center of the crater.

The 3D spatial distribution in Fig. 1(a) presents circular contours in accordance with our Gaussian laser beam. This crater has an inner diameter of 160 μm and a central depth of 2.5 μm, which indicates important matter removal. Along the profile in Fig. 1(b), the crater resembles a Gaussian curve except that a rim surrounds the crater. This wavy aspect of the edge is imputed to some heated silica moving away from the hottest zone, and the rippling aspect is formed by surface-tension gradients generated by temperature gradients [19]. For silica, this rim reaches variable heights that can be several micrometers depending on conditions of irradiation [20]. Thus, its contribution to the propagation of the laser beam could be important.

B. Maxwell Approach

The first stage of this study was the computation, using a numerical code that solves Maxwell equations in the time domain, of the perturbation induced on a plane wave by the MD_{test}. For the propagation direction z, this perturbation will be characterized by a factor $F_{MW} = a(x, y) \cdot \exp(i\varphi(x, y))$ modifying the plane wave electric field in the (x, y) plane, where a and φ are the amplitude and the phase of this factor, respectively. The dimensions of the computation domain were 500 μm in the x directions, 500 μm in the y direction, and 5 μm in the z direction. The 5 μm in the z direction is decomposed in 1 μm of air and 4 μm of fused silica. The boundary between air and fused silica is modified to include the MD_{test} profile. The mesh is defined with 400 points on the x or y axis and 1000 points in the z direction. In order to verify the stability condition, 5000 time steps of 1.6×10^{-17} s were necessary. To simulate a continuous wave, a quasi-steady state at the end of the computation is needed, which is obtained using a smoothed Heaviside time profile with a rise time of 10 fs.

The perturbation factor (F) we look for is a complex number, while Maxwell equations in the time domain are real equations. To recover the electric field envelope amplitude and phase inside fused silica, two runs have been performed, one with a sine wave and the other with a cosine wave. The computed amplitude $a(x, y)$ and phase $\phi(x, y)$ for the perturbation factor induced by the MD_{test} are shown in Fig. 2, in the case of the wavelength $\lambda = 355$ nm.

Although the computation is 3D, the axi-symmetric character of the perturbation is preserved. This result indicates that the amplitude could be taken as equal to one because it remains always close to this value. Moreover, by comparing the phase with the MD_{test} profile shown in Fig. 1, we observe a notable similarity between both curves. The small angles of incidence of the plane wave on the MD_{test} surface explain this

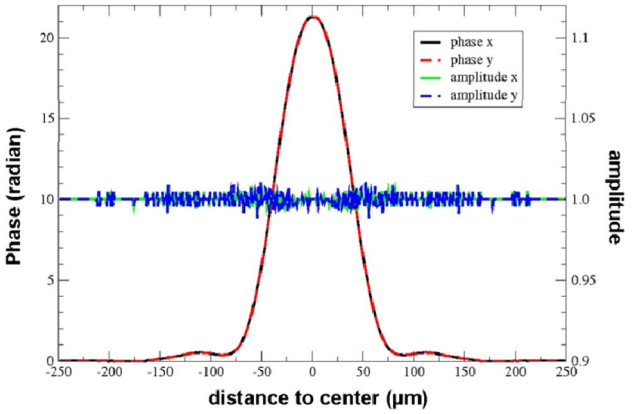

Fig. 2. Amplitude (right scale) and phase (left scale) for the MD_{test} perturbation factor obtained with a Maxwell 3D computation. To check the axi-symmetry, the results in the x and y directions are plotted.

result. This step is important because this similarity is not always verified.

C. Axi-Symmetric Approach

In the second stage, we introduce the MD_{test} perturbation factor in an axi-symmetric code solving the 1D transverse propagation equation:

$$\frac{\partial A}{\partial z}+\frac{1}{2ik_0}\left(\frac{\partial^2 A}{\partial \rho^2}+\frac{1}{\rho}\frac{\partial A}{\partial \rho}\right)=0, \tag{1}$$

where A is the laser beam envelope, k_0 is the wavenumber at the frequency we use, z is the abscissa on the propagation axis, and ρ is the radius in the transverse plane. The interface between air and silica corresponds to $z=0$. The Crank–Nicolson discretization method [21] is used with a solver based on an LU-type decomposition method [22]. The advantages of this approach are its simplicity and aptitude to follow step by step the wave evolution inside fused silica and not only at a few positions. Such a calculation is well adapted to propagation in air and/or a fused silica component for which the perturbed domain stays relatively small. This corresponds to a propagation of a few millimeters. For longer propagation, the 2D transverse approach described below has to be used.

From the Maxwell calculation, we have defined the factor of perturbation F_{MW} corresponding to the MD_{test}. Taking a plane wave as the initial wave, we calculate its propagation solving Eq. (1). Then, this simulation is compared with three different perturbation factors:

1) $F'_{MW}=F_{MW}/a(x,y)$, i.e., the amplitude variation is neglected
2) F_{EXP}, i.e., the phase is described from the experimental profile
3) F_{GAUSS}, i.e., the phase is defined by a Gaussian

The factor F'_{MW} is obtained by fixing $a=1$ in the Maxwell simulation, and only the phase will drive the propagation. The F_{EXP} is given by again $a=1$ and with the phase depending on the experimental profile (profil(ρ)) through the formula $\varphi(\rho)=2\pi/\lambda(n_{SiO_2}-1)\cdot \text{profil}(\rho)$, where λ is the wavelength and n_{SiO_2} is the silica refractive index. The F_{GAUSS} is also defined by $a=1$ and $\varphi(\rho)$ from the formula above but with a Gaussian profile approaching the experimental one. For each factor of perturbation, we calculate the coefficient C_{NUM} along the axis of propagation. This factor corresponds to the maximum (with respect to ρ) of the ratio between the UV laser beam fluence at a distance z and its fluence at $z=0$. Simulations realized for the four different perturbation factors are compared in Fig. 3.

The evolution of C_{NUM} as the function of z shows that quasi-identical evolution is obtained using the factors of perturbation F_{MW}, F'_{MW}, or F_{EXP}. Thus, the amplitude simplification ($a=1$) has no consequence. Moreover, the Maxwell computation is not necessary to define an MD factor, since the F_{EXP} gives again the same result, although it is described directly from the experimental profile. On the other hand, the Gaussian profile results are quite different from the others. As a consequence, a precise experimental data profile is necessary to obtain a valid estimation for the laser beam evolution. A second series of computations were run in order to check the impact of the mesh size in our numerical approach. We found a convergence using 4096 points in the ρ direction (as used in Fig. 3).

D. Two-Dimension Transverse Approach

In order to take into account more realistic profiles, a 2D transverse approach has been developed. Thus, we consider the envelope equation:

$$\frac{\partial A}{\partial z}+\frac{1}{2ik_0}\left(\frac{\partial^2 A}{\partial x^2}+\frac{\partial^2 A}{\partial y^2}\right)=0, \tag{2}$$

where x and y are the coordinates in the transverse plane. Its resolution is based on a spectral method similar to the one used for laser beam focusing [23]. Equation (2) is, thus, solved in the Fourier space, where A is the electric field envelope including the MD_{test} experimental phase factor (F_{EXP}). In the case of a plane wave, we consider only the perturbative part of the electric field. Thus, the Fourier transform of the initial envelope is multiplied by the propagation phase term. Then, the solution is given by applying the inverse Fourier transform to this product. The propagation phase term is not integrable; nevertheless, it has a Fourier transform (in the distribution sense) that is again a function. Therefore,

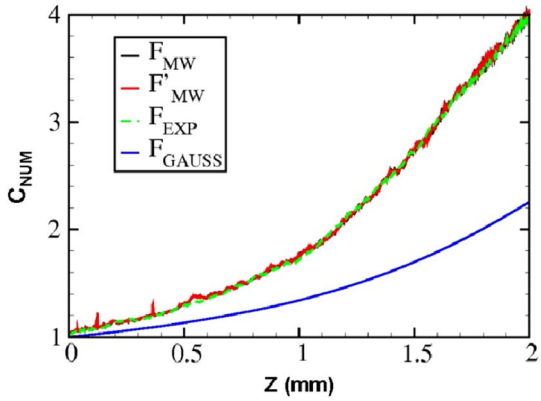

Fig. 3. Evolution of the relative fluence maximum as a function of the distance for perturbation factors: F_{MW} (black line), F'_{MW} (red line), F_{EXP} (green dashed line), F_{GAUSS} (blue line).

the solution can also be defined as the convolution product of the initial envelope with this function. Finally, this convolution product is rewritten as the Fourier transform of the initial envelope with two multiplicative factors, one before and one after the Fourier transform:

$$A(a,b,z) = -i\frac{k_0}{z}e^{-i\frac{k_0}{2z}(a^2+b^2)}\mathrm{TF}\left[A(x,y,0)e^{-i\frac{k_0}{2z}(x^2+y^2)}\right]\left(\frac{k_0}{z}a,\frac{k_0}{z}b\right). \tag{3}$$

The advantage of such an approach is that, thanks to the factor k_0/z, the solution at a given distance z is directly defined on the complete area that the diffracted wave occupies. The drawback is that for short propagation this factor is very large, and it is recommended to use the classical method with two Fourier transforms.

Different mesh sizes have been tested to evaluate the convergence of the method. It has been established that 4096 points in the x and y axis give satisfaction. To verify this convergence, we compared runs using 4096 or 8192 points. To complete the study, these simulations were done using the 1D transverse method as well as the 2D transverse method, always from the MD_{test}. Results after 2 mm of propagation are shown in Fig. 4, together with a 1D transverse calculation using the phase defined by a Gaussian with 4096 points.

The figure shows clearly that for both 1D and 2D methods the results are identical to those obtained using 4096 or 8192 points for the mesh sizes. This confirms that the convergence is reached with 4096 points. Moreover, 2D and 1D computations have given the same results. Then, we will use the 1D transverse approach with 4096 points to model our experiment. Nevertheless, for longer propagation distances than the 2 mm used in this study, 1D calculations require too much time, and the 2D code will then be better suited. On the other hand, using the Gaussian approximation (F_{GAUSS}) for the factor of perturbation, results (blue line in Fig. 4) agree with the other results for the C_{NUM} maximum localization (80 μm from the center) but are notably different for evaluating this maximum value (2.25 instead of 3.95). This corroborates previous results shown in Fig. 3. For easy comparison with experiments, we note $\varnothing_{NUM} = 160$ μm the diameter of this zone linked to the maximum of C_{NUM}, where important perturbations are expected.

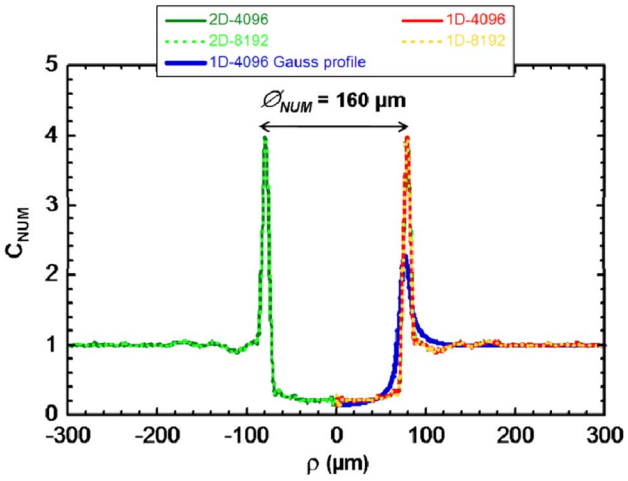

Fig. 4. Relative fluence as a function of the location to the MD_{test} center. Five calculations are compared at $z = 2$ mm: a 2D with a crude mesh (dark green line), a 2D with a fine mesh (green dotted line), a 1D with a crude mesh (red line), a 1D with a fine mesh (yellow dotted line), and a 1D with a crude mesh from Gaussian defect (blue line).

E. Case of Gaussian Beam Illumination

As detailed in the next session, experiments were conducted using a Gaussian beam with transverse dimensions of the same magnitude as the crater size. Therefore, calculations were performed both to investigate this specific case of irradiation and to compare with the case of a planar wave. A series of 16 computations with the factor of perturbation F_{EXP} were run to study the influence, on the propagation, of the UV laser beam position (ρ_{beam}) from the MD_{test} center. To take into account such a shift in the radial direction, we model the UV laser beam with a Gaussian profile ($1/e^2$ at 300 μm) centered on ρ_{beam}. As our calculations are 1D, the axi-symmetrical geometry is described by a laser beam in the form of a torus. Comparison between computations realized with this configuration or with the 2D transverse pattern, describes in the next part, shows negligible difference for the maximum fluence at the back surface. The first run with $\rho_{beam} = 0$ coincides with the truly Gaussian beam center on the MD_{test}. For the next runs, the beam is moved at each time 10 μm further away from the center. Results of C_{NUM} after 2 mm of propagation as a function of ρ_{beam} are shown in Fig. 5, together with the calculation for a plane wave with fluence equal to the maximum of the Gaussian wave.

The toroidal wave exhibits a maximal coefficient $C_{NUM} = 3.95$ at $\rho_{beam} = 65$ μm, which corresponds to a beam centered inside the crater close to the MD_{test} rim [Fig. 1(b)]. Moreover, this maximum is close to the value obtained with the plane wave related to the maximum of the Gaussian fluence. It is notable that a plane wave has nearly the same effect as a Gaussian wave optimally placed on the MD_{test}. Therefore, we will consider only 1D calculations with the plane wave for comparison between experiment and simulations.

From the developments of Section 2, a numerical approach enables us to estimate rapidly the impact of fused silica surface defects on the UV laser beam propagation. In that

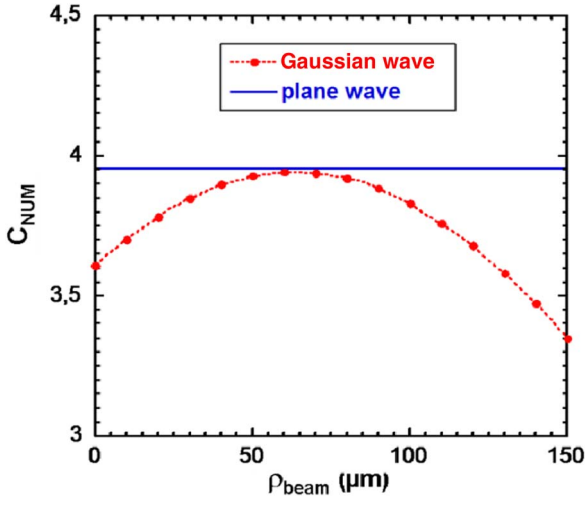

Fig. 5. Effect of UV laser displacement (ρ_{beam}) on the relative fluence maximum (C_{NUM}).

way, we represent the evolution of the coefficient C_{NUM} along the z axis as a function of the radius in the transverse plane ρ. The 3D image of such a calculation with MD_{test} using the factor of perturbation F_{EXP} is shown in Fig. 6. We can easily follow the evolution of the maximum of C_{NUM} together with its transversal position ($\varnothing_{NUM}$). Moreover, on the front surface (at $z = 0$ mm), the region mainly contributing to the overintensification is distinguishable ($\rho = 40$–80 μm), which is in good accordance with the previously determined $\rho_{beam} = 65$ μm (Fig. 5). Although these calculations are useful for estimating the upper limit for the fluence to be involved at the rear surface of silica (at $z = 2$ mm), the ultimate test must be based on the laser damage response.

3. EXPERIMENTAL PROCEDURE

In order to compare simulation results to experimental ones, craters with different profiles were created on fused silica samples. All samples were Suprasil 312 (from Heraeus) and polished by THALES-SESO using a "super polishing" technology. These 25 mm diameter and 2 mm thick samples were irradiated with different CO_2 laser pulse durations, from 100 ms to 1 s. The power on the sample front surface was varied between 5 and 7 W. All sites were then characterized by white light interferometry. For each set of parameters, the profile crossing the crater center has been extracted from the 3D map.

Damage test experiments were performed using a frequency-tripled Nd:YAG laser operating at a wavelength of 355 nm [24]. A laser diode seeder ensures that the temporal profile is a single longitudinal mode and stable shot-to-shot; the equivalent pulse duration (defined as the ratio of the total energy to peak power) was 2.5 ns. A convex lens whose focal length is approximately 5 m focuses the beam. In this configuration, the spatial profile is Gaussian with a diameter of 0.6 mm at $1/e$ on the sample surface, and the depth of focus is longer than the sample thickness, ensuring a constant beam shape along the propagation in the bulk. All tests were made at normal incidence using linear polarization. The fluence is determined within an error of as much as ±10% [25].

For the present study, we used a mobile sample holder supporting each silica substrate vertically with MDs located on the input face (i.e., toward the incoming laser beam) and carried out tests with the classical one-on-one procedure (1/1) [26,27]. More precisely, the experiment was realized by exposing each MD to a single shot at a given fluence. A distance of 3 mm was used between MDs in order to avoid collateral site-to-site effects. Also, the beam diameter, including more than 80% of the maximum fluence (about 250 μm), is smaller than the MD. To take into account the reduced size of the UV laser beam and that the intensification maximum is expected when the beam is centered at the proximity of the MD border (as shown in Figs. 4 and 6), we translated the component to specifically irradiate the crater edge. Nevertheless, the spatial profile has been recorded for each shot to determine the exact peak fluence (F_{max}) and beam position on the corresponding MD to test. An accurate determination of the local energy distribution on the whole MD was then obtained. Such a test configuration is illustrated in Fig. 7 for the MD_{test} site. Finally, after UV laser irradiation, the damage event was assessed by inspection of the optical component rear surface by means of a long working microscope. This allows us to accurately localize the damage and its shape.

In order to illustrate the method and the results obtained, we report here the specific case of irradiations on several MDs quasi-identical to the MD_{test} site (realized with the same parameters of the CO_2 laser and then noted also MD_{test}). A preliminary test with the 1/1 procedure was performed on bare silica. Damage sites created on the rear face of this component were detected, and the 50% damage probability was determined and chosen as the reference for our experiments: $F_{BS\text{-}50\%} = 21.5 \pm 0.5$ J/cm^2. After irradiations on several MD_{test} at such a value of fluence, very large damage has been systematically observed on the rear face leading to a 100% damage probability. These first results were proof of light intensification on the rear surface. By strongly reducing the fluence, we have still obtained damage events but much smaller and following a ring pattern, as the example

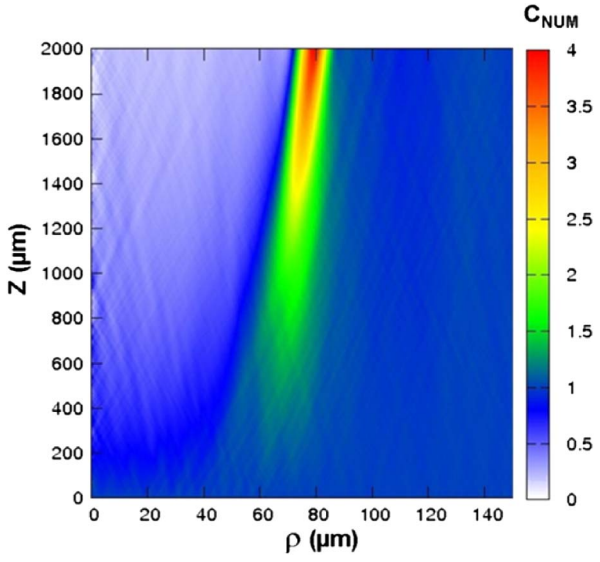

Fig. 6. Calculation for the MD_{test} defect irradiated with a plane wave at the wavelength of 355 nm. 3D map of the coefficient C_{NUM} as a function of the distance of propagation (z axis) and the distance from the center of the defect (ρ axis).

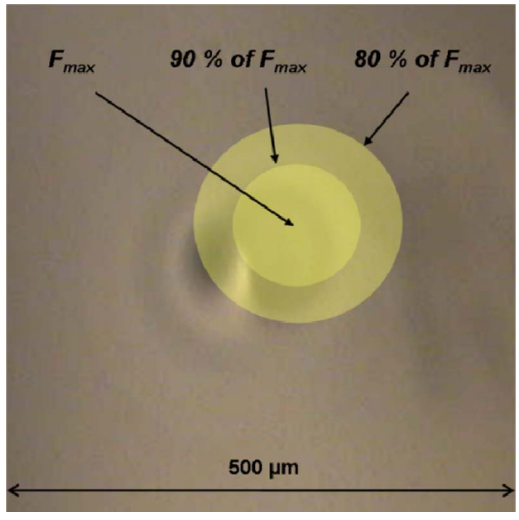

Fig. 7. Nomarski image of the MD_{test} site on the front side of the samples (CO_2 laser during 100 ms with a power of 5.3 W) including the representation of the Nd:YAG laser location for tests (yellow disk).

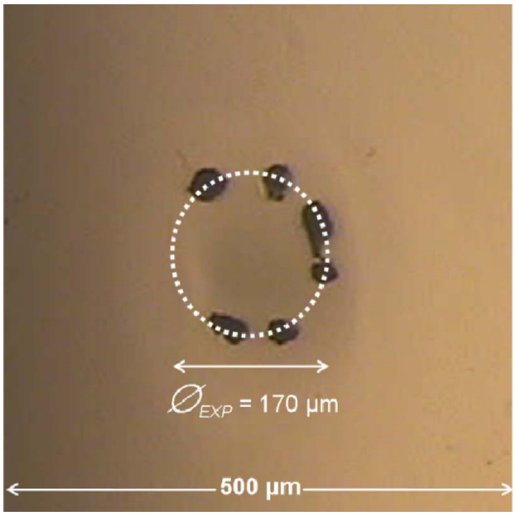

Fig. 8. Nomarski image of the sample on the backside after irradiation of the MD_{test} site with $F_{max} = 14$ J/cm^2.

shown in Fig. 8 for a fluence of 14 J/cm^2. In this figure, we observe damage resulting from several pinpoints located in a circular region, although it results from a single irradiation. A dotted circle whose diameter is $\varnothing_{EXP} = 170$ μm marks this zone. Moreover, no damage appears in the area corresponding to the central zone of the UV laser irradiation where the fluence is the highest. This result clearly indicates the much more important contribution played by the circumferential region of the MD_{test} compared to its central part.

To quantify the light amplification factor due to the MD_{test} profile by using the test configuration described in Fig. 7, fluences have been progressively decreased on new similar sites. At each fluence, irradiations were repeated on a series of MD_{test}, and damage sites were detected or not detected on the rear surface to evaluate the laser damage probability. More specifically, the fluence associated to the 50% probability has been determined and found to be $F_{MD\text{-}50\%} = 6 \pm 1$ J/cm^2. Therefore, this fluence is compared to that obtained on the bare substrate, and the ratio between these two values permits us to define an experimental factor of amplification: $C_{EXP} = F_{BS\text{-}50\%}/F_{MD\text{-}50\%}$. We then conclude that the fused silica surface defect defined as MD_{test} modifies the UV laser beam propagation by a factor $C_{EXP} = [3.0–4.4]$ enclosed in a circular region whose diameter is $\varnothing_{EXP} = 170$ μm.

To go further, irradiations have been carried out on numerous experimental defects characterized by various diameters, depths, and rims. In this way, several $F_{MD\text{-}50\%}$ have then been measured and compared to the predetermined $F_{BS\text{-}50\%}$, leading in each case to an amplification factor related to the associated MD. The corresponding region of damage sites is also observed, which indicates the presence of one or several annular patterns. Experimental and computational factors (C_{EXP} & C_{NUM}) and diameters ($\varnothing_{EXP}$ & $\varnothing_{NUM}$) are compared and discussed in the next section.

4. COMPARISON OF CALCULATIONS WITH EXPERIMENTS

To begin the comparison, we first consider the MD_{test} profile extensively described above for numerical calculations and experiments. From calculations, we found $C_{NUM} = 3.95$ and $\varnothing_{NUM} = 160$ μm and, from the damage test, $C_{EXP} = [3.0–4.4]$ and $\varnothing_{EXP} = 170$ μm. This remarkable concordance between our code and the experiment is obtained thanks to the specifically adapted experimental procedure. Moreover, the utilization of a 50% damage probability as the reference for our experiments gives us much more precision for the determination of the intensification factor. On this basis, we next duplicated the same protocol with different types of MD, notably with greater crater depths.

Other series of identical MDs realized with the CO_2 laser power of 6.5 W during 100 ms have been investigated. For this new set of parameters, a typical profile crossing the deepest zone is shown in Fig. 9(a). The crater resembles a Gaussian curve with an inner diameter of 200 μm and a central depth of 16 μm. The matter removal is big and surrounded by a circular rise with a wavy aspect. Calculations with this MD profile were done with a plane wave at the wavelength of 355 nm and the factor of perturbation F_{EXP}. Results all along the propagation of 2 mm are shown in Fig. 9(b). Since the rim of this MD defect is several hundred nanometers high, its contribution to the propagation of the laser beam is essential, and a coefficient of $C_{NUM} = 12$ is reached at $z = 0.4$ mm. As before for the MD_{test} (Fig. 6), the most influent region on the front surface (at $z = 0$ mm) is visible, and it allows us to determine $\rho_{beam} = 100$ μm, which corresponds again to a beam centered slightly inside the crater close to the edge. After 2 mm of propagation, a side view of these calculations (red curve) more precisely exhibits that the coefficient C_{NUM} has several maxima in the range [3.0–3.3]. Their locations are compared with experimental results in Fig. 9(c). For the latter, the MD site has been irradiated with the UV laser at fluence 12 J/cm^2. The resulting damage contains several pinpoints located in three circular regions (white dotted circles) indicating that $\varnothing_{EXP} = 250$, 320, and 410 μm. If we identify $\varnothing_{NUM}$ for each peak where $C_{NUM} \geq 3.0$, a very good accord is observed with experiment. Following the procedure defined above, irradiations were repeated on a series of similar MD at different fluences, and the laser fluence whose damage probability is 50% was then evaluated. It was found to be $F_{MD\text{-}50\%} = 7 \pm 1$ J/cm^2. Therefore, the fused silica surface defect MD defined by the profile in Fig. 9(a) modifies the UV laser beam propagation by a factor $C_{EXP} = [2.6–3.6]$. These values enclose C_{NUM} confirming the good prediction of our calculation.

To verify the influence on propagation of the UV laser beam position (ρ_{beam}) from the MD center, we realized a series of fresh MDs with wider and deeper profiles. For this purpose, the CO_2 laser was operated during 1 s instead of 100 ms with a power of 5.5 W. The crater profile (not shown here) resembles a Gaussian curve with an inner diameter of 280 μm surrounded by very large rim and a central depth of 48 μm. A sequence of computations using the same UV laser model as for calculations with the MD_{test} (Fig. 5) has been run to compute C_{NUM} as a function of ρ_{beam}. Results after 2 mm of propagation are shown in Fig. 10, together with calculation for a plane wave with fluence equal to the maximum of the Gaussian wave. The maximal $C_{NUM} = 5.5$ corresponds to $\rho_{beam} = 170$ μm, which is centered approximately at the higher edge. For the damage test, we irradiated all MD sites with the UV laser at 5 J/cm^2, and then $F_{max} = 27.5$ J/cm^2. The first trial with $\rho_{beam} = 0$ coincided with the laser beam center on each MD, and a damage probability is established

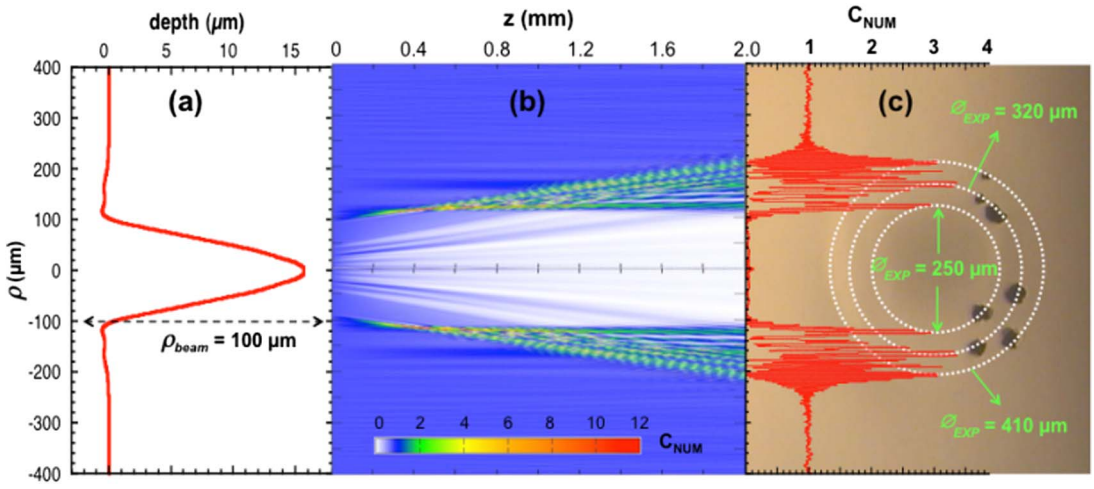

Fig. 9. (a) Profile by interferential microscopy of a site heated during 100 ms with a CO_2 laser power of 6.5 W. (b) 3D map of the coefficient C_{NUM} as a function of the distance of propagation (z axis) and the distance from the center of the defect (ρ axis). (c) Nomarski image of the sample backside after UV irradiation with $F_{max} = 12$ J/cm^2, together with the coefficient C_{NUM} as a function of the distance from the center of the defect (ρ axis).

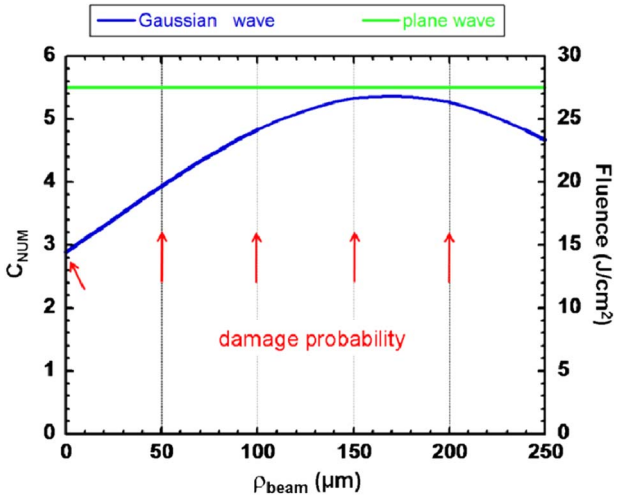

Fig. 10. Calculations of C_{NUM} after 2 mm of UV laser propagation as a function of the distance from the MD center, for both Gaussian (blue) and planar (green) waves. For damage test done with equivalent MDs, probabilities are shown at the location of the irradiation (red arrow).

after irradiation of 10 or more spots (irradiations recorded with a shift ≥20 μm were not considered). For the next runs, the beam was moved at each time 50 μm further away from the center, allowing us to evaluate the damage probability at a different ρ_{beam}. These values indicated in Fig. 10 are consistent with the location near $\rho_{beam} = 70$ μm of the 50% damage for the bare silica ($F_{BS\text{-}50\%} = 21.5$ J/cm^2).

To complete these observations, calculations with an l MD site identical to that of the preceding series were done with a plane wave at the wavelength of 355 nm and the factor of perturbation F_{EXP}. Results all along the propagation of 2 mm are shown in Fig. 11(a). As the rim of this MD defect is several micrometers high, it generates rapidly around $z = 0.35$ mm a very high focalization at $\rho = 150$ μm matching with a coefficient $C_{NUM} = 30$. Again, the region mainly contributing to the overintensification on the front surface (at $z = 0$ mm) is well marked, and we determine $\rho_{beam} = 120 \pm 20$ μm, which corresponds once more to the inner crater edge (140 μm). We discern that the coefficient C_{NUM}, after 2 mm of propagation, has many repetitive values ≥2 delimited by two limits at $\varnothing_{NUM} =$ 340 and 760 μm, with $C_{NUM} = 5.5$ and 3, respectively. This

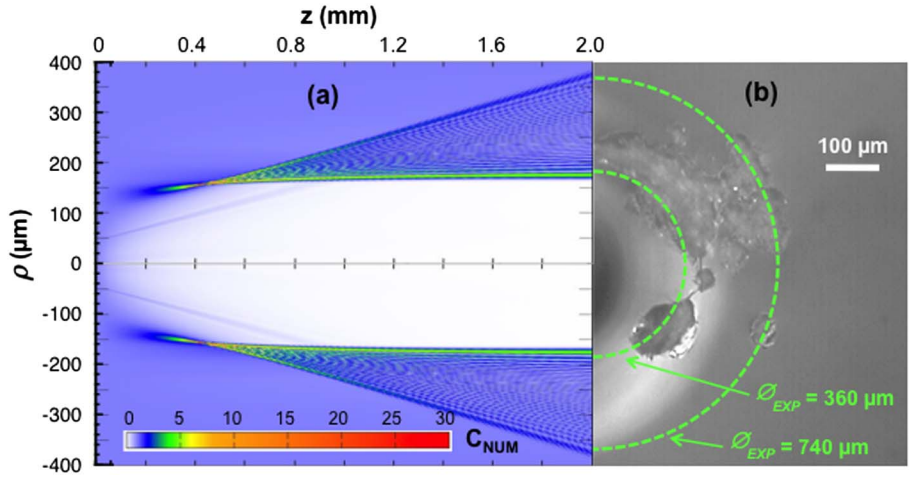

Fig. 11. (a) For a site heated during 1 s with a CO_2 laser power of 5.5 W, 3D map of the coefficient C_{NUM} as a function of the distance of propagation (z axis) and the distance from the center of the defect (ρ axis). (b) Nomarski image of the sample backside after UV irradiation with $F_{max} = 15$ J/cm^2.

Table 1. Calculations and Experimental Results for Five Distinct MDs Realized with Different Parameters of the CO_2 Laser

Parameters of CO_2 Laser	MD: Depth & Diameter	$\varnothing_{NUM}$(μm)	C_{NUM}	$\varnothing_{EXP}$(μm)	C_{EXP}
600 μm/100 ms/5.0 W	1 μm/ 130 μm	130	1.4	130	1.1–1.4
600 μm/100 ms/5.3 W	2 μm/130 μm	160	3.95	170	3.0–4.4
600 μm/100 ms/6.5 W	16 μm/200 μm	250–410	3.0–3.3	250–410	2.6–3.7
600 μm/200 ms/5.9 W	25 μm/230 μm	340–510	3.5–4.0	330–510	3.2–4.0
600 μm/1000 ms/5.5 W	48 μm/280 μm	350–750	5.3–5.5	360–740	4.7–6.3

calculation is compared with experimental results in the case of an MD irradiated with the UV laser at fluence 15 J/cm^2. As a consequence of such high fluence, the resulting damage is very large. But this latter is well delimited by two series of big pinpoints (green dotted circles) related to $\varnothing_{EXP} = 360$ and 740 μm, as shown in Fig. 11(b). Although widespread damage is usually difficult to analyze, these measurements confirm forcefully the good prediction of our calculation.

Finally, we resume our study using MDs realized with a CO_2 laser (Table 1). Five different sets of parameters have been used to produce MDs for which profiles varied from 1 to 48 μm in depth and 130 to 280 μm in diameter. For each MD we have evaluated, both numerically and experimentally, the diameter ∅ where damage initiated and the amplification factor C. We note that for largest craters, damage sites are located on large areas that correspond to ranges of ∅ linked to ranges of C. Very good accord between experiments and our calculation is obtained for all MDs. More precisely, the difference for ∅ is of the order of the measurement inaccuracy, and the values of C_{NUM} are always included in the corresponding C_{EXP} range. By increasing our statistic, we could reduce the $F_{MD\text{-}50\%}$ incertitude and then expect to find better agreement between C_{NUM} and C_{EXP}.

5. CONCLUSION

Modulation of the laser intensity caused by surface defects on optical components plays an important role in the laser wave propagation. Several numerical tools are used to understand the impact of different defects as laser damage, contamination, or mitigation. We have developed a numerical approach based on three codes for evaluating the diffraction pattern resulting from a defect and its consequences on downstream propagation. The defect that is characterized by its geometry and its optical properties modifies the laser electromagnetic field. We have quantified this modification with a perturbation factor. The first code solves the full 3D Maxwell equations in order to determine the consequences of the defect on the laser beam intensity and phase. Such a code needs very large memory and computation time. Thus, although it permits us to compute the perturbation factor directly from the defect geometry and optical properties, it cannot be used for long propagation. Therefore, the influence of the defect on the laser beam is computed with a simpler propagation code solving the Schrödinger equation. For axi-symmetric defects, the 1D transverse numerical code computes the laser field with a precise resolution step by step along the propagation. In complement, for 3D defects a 2D transverse numerical code using Fourier transform computes the diffraction pattern. Moreover, this code is appropriate for very long propagation distances, since it can compute the laser field directly at any distance. The computations with these two last codes define the position and value of the laser field intensity maximum.

In order to compare simulation results to experimental ones, specific defects were created on fused silica by CO_2 laser irradiation. Although the numerical method could be applied to more complex defects, we have limited our study to smooth defects. These defects were localized at the front face to evaluate their consequences on the rear surface when a laser beam crosses this optical component. The damage tests at sufficiently high fluence directly give the position of the laser field intensity maximum. We have also determined an experimental amplification factor by comparing the 50% damage probability evaluated with the defect to the 50% damage probability on bare silica. Good agreement has been found between the experimental and the numerical amplification factors and also between the damage location and the position of the numerical intensity maximum. This study has been carried out on different kind of defects to fully validate the numerical approach. This work shows also that if the factor of perturbation is just defined by a Gaussian profile approximating the experimental one, good agreement is found for the damage position, but strong undervaluation of the numerical amplification factor compared to the experimental one can be observed. By considering a factor of perturbation whose amplitude is no longer equal to 1 or whose phase is no longer directly proportional to the profile, the method introduced here allows the study of more general defects.

REFERENCES

1. S. Palmier, L. Gallais, M. Commandré, P. Cormont, R. Courchinoux, L. Lamaignère, J. L. Rullier, and P. Legros, "Optimization of a laser mitigation process in damaged fused silica," Appl. Surf. Sci. **255**, 5532–5536 (2009).
2. S. T. Yang, M. J. Matthews, S. Elhadj, D. Cooke, G. M. Guss, V. G. Draggoo, and P. J. Wegner, "Comparing the use of mid-infrared versus far-infrared lasers for mitigating damage growth on fused silica," Appl. Opt. **49**, 2606–2616 (2010).
3. I. L. Bass, G. M. Guss, M. J. Nostrand, and P. J. Wegner, "An improved method of mitigating laser induced surface damage growth in fused silica using a rastered, pulsed CO_2 laser," Proc. SPIE **7842**, 784220 (2010).
4. W. Dai, X. Xiang, Y. Jiang, H. J. Wang, X. B. Li, X. D. Yuan, W. G. Zheng, H. B. Lv, and X. T. Zu, "Surface evolution and laser damage resistance of CO_2 laser irradiated area of fused silica," Opt. Lasers Eng. **49**, 273–280 (2011).
5. B. Bertussi, P. Cormont, S. Palmier, P. Legros, and J. L. Rullier, "Initiation of laser-induced damage sites in fused silica optical components," Opt. Express **17**, 11469 (2009).
6. L. Gallais, P. Cormont, and J. L. Rullier, "Investigation of stress induced by CO_2 laser processing of fused silica optics for laser damage growth mitigation," Opt. Express **17**, 23488 (2009).
7. P. Cormont, L. Gallais, L. Lamaignère, J. L. Rullier, P. Combis, and D. Hebert, "Impact of two CO_2 laser heatings for damage repairing on fused silica surface," Opt. Express **18**, 26068 (2010).
8. L. Robin, P. Combis, Ph. Cormont, L. Gallais, D. Hebert, Ch. Mainfray, and J. L. Rullier, "Infrared thermometry and

interferential microscopy for analysis of crater formation at the surface of fused silica under CO_2 laser irradiation," J. Appl. Phys. **111**, 063106 (2012).
9. M. J. Matthews, I. L. Bass, G. M. Guss, C. C. Widmayer, and F. L. Ravizza, "Downstream intensification effects associated with CO_2 laser mitigation of fused silica," Proc. SPIE **6720**, 67200A (2007).
10. M. Runkel, R. Hawley-Fedder, C. C. Widmayer, W. Williams, C. Weinzapfel, and D. Roberts, "A system for measuring defect induced beam modulation on inertial confinement fusion-class laser optics," Proc. SPIE **5991**, 59912H (2005).
11. L. Li, X. Xiang, X.-T. Zu, H.-J. Wang, X.-D. Yuan, X.-D. Jiang, W.-G. Zheng, and W. Dai, "Numerical simulation of the modulation to incident laser by the repaired damage site in a fused silica subsurface," Chin. Phys. B **20**, 074209 (2011).
12. F. Y. Génin, A. Salleo, T. V. Pistor, and L. L. Chase, "Role of light intensification by cracks in optical breakdown on surfaces," J. Opt. Soc. Am. A **18**, 2607–2616 (2001).
13. F. Bonneau, P. Combis, A. Pujols, J. L. Rullier, M. Sesques, and J. Vierne, "Numerical simulations of laser/defect induced absorption in SiO_2," Proc. SPIE **4932**, 250–257 (2003).
14. F. Y. Génin, M. D. Feit, M. R. Kozlowski, A. M. Rubenchik, A. Salleo, and J. Yoshiyama, "Rear-surface laser damage on 355-nm silica optics owing to Fresnel diffraction on front-surface contamination particles," Appl. Opt. **39**, 3654–3663 (2000).
15. M. J. Matthews, N. Shen, J. Honig, J. D. Bude, and A. M. Rubenchik, "Phase modulation and morphological evolution associated with surface-bound particle ablation," J. Opt. Soc. Am. B **30**, 3233–3242 (2013).
16. Y. Zheng, P. Ma, H. Li, Z. Liu, and S. Chen, "Studies on transmitted beam modulation effect from laser induced damage on fused silica optics," Opt. Express **21**, 16605 (2013).
17. L. Li, X. Xang, X.-T. Zu, H.-J. Wang, X.-D. Yuan, S.-B. He, X.-D. Jiang, and W.-G. Zheng, "Incident laser modulation of a repaired damage site with a rim in fused silica rear subsurface," Chin. Phys. B **21**, 044212 (2012).
18. A. Bourgeade and B. Nkonga, "Numerical modeling of laser pulse behavior in nonlinear crystal and application to second harmonic generation," Multiscale Model. Simul. **4**, 1059–1090 (2005).
19. T. R. Anthony and H. E. Cine, "Surface rippling induced by surface-tension gradients during laser surface melting and alloying," J. Appl. Phys. **48**, 3888–3894 (1977).
20. M. J. Matthews, I. L. Bass, G. M. Guss, C. C. Widmayer, and F. L. Ravizza, "Downstream intensification effects associated with CO_2 laser mitigation of fused silica," Proc. SPIE **6720**, A7200A (2008).
21. M. Delfour, M. Fortin, and G. Payre, "Finite-difference solutions of a non-linear Schrödinger equation," J. Comput. Phys. **44**, 277–288 (1981).
22. Ph. Ciarlet, *Introduction to Numerical Linear Algebra and Optimisation*, Cambridge Texts in Applied Mathematics (Cambridge University, 1989).
23. A. Bourgeade and B. Nkonga, "Numerical simulations of the focal spot generated by a set of laser beams: LMJ," ESAIM: Proc. **32**, 1–17 (2011).
24. L. Lamaignère, G. Dupuy, T. Donval, G. Grua, and H. Bercegol, "Comparison of laser-induced surface damage density measurements with small and large beams: toward representativeness," Appl. Opt. **50**, 441–446 (2011).
25. L. Lamaignère, M. Balas, R. Courchinoux, T. Donval, J.-C. Poncetta, S. Reyné, B. Bertussi, and H. Bercegol, "Parametric study of laser-induced surface damage density measurements: toward reproducibility," J. Appl. Phys. **107**, 023105 (2010).
26. "Lasers and laser-related equipment: Test methods for laser-induced damage threshold. Part 1: Definitions and general principles," ISO 21254-1:2011.
27. "Lasers and laser-related equipment: Test methods for laser-induced damage threshold. Part 2: Threshold determination," ISO 21254-2:2011.